Energy Storage Materials 49 (2022) 77–84

Contents lists available at ScienceDirect

Energy Storage Materials

journal homepage: www.elsevier.com/locate/ensm

Artificial cathode electrolyte interphase for improving high voltage cycling stability of thick electrode with Co-free 5 V spinel oxides

Weikang Li[a], Diyi Cheng[b], Ryosuke Shimizu[a], Yixuan Li[a], Weiliang Yao[b], Ganesh Raghavendran[a], Minghao Zhang[a,*], Ying Shirley Meng[a,b,c,*]

[a] Department of NanoEngineering, University of California San Diego, La Jolla, CA 92093, USA
[b] Materials Science and Engineering, University of California San Diego, La Jolla, CA 92093, USA
[c] Pritzker School of Molecular Engineering, University of Chicago, Chicago, IL 60637, USA

A B S T R A C T

Spinel-type cathode $LiNi_{0.5}Mn_{1.5}O_4$ (LNMO) has intrigued the transportation industry due to its high operating voltage and total elimination of the expensive cobalt element. However, LNMO cathode with high mass loading (> 3 mAh/cm^2 in areal capacity) has suffered from excessive capacity degradation upon long cycling. Here, a robust Al_2O_3 surface layer is introduced to the thick LNMO electrode via atomic layer deposition (ALD). The capacity retention in full cells with the graphite anode is improved from 46.3% to 75.3% after 300 cycles with cutoff voltage up to 4.85 V, while enabling average Coulombic efficiency of 99.9% during the cycling. The post-mortem analyses reveal that the Al_2O_3 surface layer would convert to Al-O-F /Al-F species upon cycling, offering stable interphase to protect the cathode material. These results demonstrate the significance of surface modification enabling high voltage cathode for next-generation LIBs.

With the demand for next-generation high-end electronic devices and the popularity of electric vehicles increasing, innovative lithium-ion battery (LIB) technology has run into bottleneck issues [1]. Cathode material plays a key role when considering all components in LIBs for more than 40% in both cost and weight ratios [2,3]. The current commercialization and research for cathode materials mainly focus on lithium metal oxides ($LiNi_xCo_yMn_zO_2$, x+y+z=1, NCM) with a layered structure, lithium iron phosphate ($LiFePO_4$, LFP) with an olivine structure, and lithium manganese oxides ($LiMn_2O_4$, LMO) with spinel structure. Layered lithium metal oxides have high energy densities, but the use of expensive and toxic cobalt elements greatly restricts their application in the widespread commercialization of electric vehicles [4]. Cathode materials without Co element, such as LFP and LMO, offer limited energy density, lower than 500 Wh/kg at the material level, which is insufficient for next-generation electric vehicles [5]. Co-free Li-rich layered oxide has also attracted extensive attention due to its high energy density, while the inferior reversibility at the material level due to the oxygen loss is yet to be fully understood [6].

In this context, a spinel-type oxide $LiNi_{0.5}Mn_{1.5}O_4$ (LNMO) obtained from LMO using proper nickel substitution has attracted extensive attention since the average working voltage can be increased from 4 V to 4.7 V [7]. The energy density for this type of spinel material can thus be significantly improved to 620 Wh/kg at the cathode material level, which is close to the classical layered oxide like NCM111. Crucially, it does not contain expensive cobalt, making LNMO cost-effective and suitable for power batteries and large-scale energy storage applications. However, the main obstacle to commercialization is in the stability of the cathode electrolyte interphase (CEI) [8,9]. The currently commercialized electrolyte is still dependent on the early development of the organic system, mainly based on various carbonic ester solvent combinations with $LiPF_6$ solute. The upper stable operating voltage is generally limited to 4.5 V vs. Li^+/Li [10]. When the voltage increases, such electrolytes decompose and fail to form an effective passivating layer, which deteriorates the battery cycling stability [11]. Consequently, a high areal cathode loading for this type of spinel cathode currently triggers excessive parasitic reactions; there has yet to be a design to achieve performance targets [7,12].

Engineering modifications for both cathode and electrolyte enhancements have been investigated considerably for LNMO material, including heteroatom doping, [13,14] novel electrolyte/additive design, [15–17] and surface coating [18,19] to improve interphase stability at high voltage conditions. Surface modification has been proven effective among all methods, and a well-designed artificial surface layer is electronically insulating to mitigate parasitic reactions between the electrode and electrolyte. Different surface modification materials have also been applied, such as conductive carbon, [20] oxides, [21] fluorides, [22] and phosphates [23]. Atomic layer deposition (ALD) is one of the most effective surface modification methods to achieve the uniform artificial layer. In each ALD cycle, the precursor molecule reacts with the substrate surface in a self-limiting way, ensuring monolayer adsorption on the target surface [24]. The ALD cycle can then be performed multiple times to control the surface layer thickness. The ALD surface modification strategy has been widely applied to various battery materials, including $LiCoO_2$ (LCO), [25,26] LMO, [27,28] NCM, [29,30] and Li-rich

* Corresponding Authors.
E-mail addresses: miz016@eng.ucsd.edu (M. Zhang), shmeng@ucsd.edu (Y.S. Meng).

https://doi.org/10.1016/j.ensm.2022.04.002
Received 11 January 2022; Received in revised form 23 March 2022; Accepted 2 April 2022
Available online 4 April 2022

Table 1
Literature summary of ALD modified LNMO for LIBs.

Year	Surface chemistry	ALD substrate	Electrode areal loading (mg/cm^2)	Cell type	Full cell cycling No.	Ending capacity of full cell(mAh/g)	Ref.
2013	Al_2O_3	Electrode	/	Half cell	/	/	[34]
2014	Al_2O_3	Electrode	/	Half cell	/	/	[35]
2015	MgF_2	Powder	6.5–8	Half cell	/	/	[36]
2015	TiO_2/ Al_2O_3	Electrode	<1	Half cell	/	/	[37]
2015	$FePO_4$	Powder	/	Half cell	/	/	[38]
2017	Al_2O_3	Electrode	/	Half cell	/	/	[39]
2017	TiO_2	Powder	/	Half cell	/	/	[40]
2019	FeO_x	Powder	25	Half cell	/	/	[41]
2020	LiF	Powder	8-13	Half cell	/	/	[42]
2013	Al_2O_3	Electrode	/	**Full cell with graphite**	100	~40	[43]
2014	$LiAlO_2$	Powder	9-10	**Full cell with graphite**	45	~90	[44]
2015	Al_2O_3	Powder	5.5	Full cell with $Li_4Ti_5O_{12}$	200	~110	[45]
2018	AlF_3	Powder	20	**Full cell with graphite**	180	~90	[46]
2021	FeO_x	Powder	3.5	Full cell with $Li_4Ti_5O_{12}$	200	~105	[47]
This work	**Al_2O_3**	**Electrode**	**22**	**Full cell with graphite**	**300**	**~80**	

layered oxide (LRLO) [31,32]. It is widely demonstrated that the artificial surface layer can significantly improve cell cycling stability due to the superior interphase resistibility towards electrolyte corrosion.

It is worth noting that the ALD process can be applied on either the active material powders or directly on the electrode [33]. For battery applications, a direct ALD process on the electrode is preferred since the electronic pathway (surface contact between the active material and the conductive additive) will not be deteriorated. Another advantage of the direct ALD process on the electrode is related to inactive components protection. Both conductive agent and binder are critical to achieving stable high voltage cycling, which is yet to be further investigated. With the rising demand for high energy density batteries, thick electrode with large areal mass loading needs to be implemented. In principle, the ALD precursors are gaseous, and their penetration through the entire thick electrode should be feasible. However, the feasibility of direct ALD modification on thick electrodes (> 20 mg/cm^2 areal mass loading) has not been investigated, especially in the full cell setup. A literature summary for ALD surface modification on different cathode materials is shown in Table 1. The cell performances were evaluated in half cells with low areal mass loading. Two key questions need to be tackled for the ALD modification on the thick electrode: (1) Is the artificial surface layer uniform along the electrode thickness direction? (2) Is there any morphological or chemical change of the artificial surface layer after long-term electrochemical cycling, especially under the high voltage cycling conditions?

In this work, we demonstrate that the ALD surface modification strategy is feasible for a thick LNMO electrode (active material areal mass ≥ 22 mg/cm^2). Aluminum oxide (Al_2O_3) was selected as the artificial surface material in this study due to its chemical stability under high voltage operation. The uniformity and the existence of the artificial surface layer after long-term cycling are revealed based on analytical electron microscopy. The ALD surface-modified LNMO cathode exhibits improved cycling performance in the full cell using graphite as the anode. It is found that the Al_2O_3 surface layer will be fluorinated after long-term cycling. The formed Al-O-F species resist acidic electrolyte corrosion, and the transition metal (TM) dissolution and redeposition are therefore mitigated. These results explicitly demonstrate the significance of CEI stability for high voltage operation.

The ALD process was directly applied on the LNMO thick electrode (~3 mAh/cm^2 in capacity loading, ~90 μm in thickness), and the designed thickness of the Al_2O_3 surface layer was 3 nm (30 ALD cycles). To verify the Al_2O_3 surface layer uniformity, lamellas from both the top and bottom locations of the ALD modified electrode were prepared by the FIB lift-out process, as shown in Fig. 1(a) and (b). The prepared lamellas were then thinned down to ~100 nm thick for STEM-EDS characterizations, and the morphology of the lamella is shown in Figure S1. As shown in Fig. 1(c) and (d), a uniform surface layer containing Al signal was observed on the particle from both the top and bottom locations. The artificial surface layers of the lamella from both the top and the bottom locations of the thick electrode are ~3 nm in thickness, which indicates that the LNMO particles through the whole electrode were uniformly coated during the ALD process. One more lamella sample is shown in Figure S2 for the uniformity verification. The extra Mn and Ni signal at the outer layer was from the redeposition because of the nearby LNMO removal during the thinning process. Large area SEM-EDS mapping with the extracted spectrum also shows the uniform Al signal on the surface of LNMO particles in Figure S3. The crystal structure of LNMO particles after the ALD process was also investigated via atomic-resolution STEM imaging, as shown in Figure S4. The rhomboid shape of the white spots implies the well-crystallized spinel structure of LNMO material viewed along the [110] zone axis. These results indicate that the ALD process has little impact on the crystalline structure of LNMO material.

The electrode's conductive agent and binder are also crucial to the cycle stability as discussed in our previous publication [5]. Herein, the carbon (SPC65) and PVDF (HSV900) from the ALD modified electrode were also checked via STEM-EDS, and the results are shown in Figure S5. Al signal can be found on both conductive agent and PVDF. The reactivity of these two inactive components towards a high-voltage environment likely decreases after ALD coating, which may contribute to less parasitic reactions and better cycling.

The unmodified and ALD-modified LNMO cathode were paired with graphite anode and assembled into full cells for the long-term cycling test. The results are shown in Fig. 2. The assembled coin cells were first cycled at C/10 twice as the formation cycles and then switched to C/3 in subsequent cycles. The discharge capacity and corresponding Coulombic efficiency are shown in Fig. 2(a). The unmodified LNMO or ALD modified LNMO electrode demonstrate more than 550 Wh/kg as the energy density at the material level from full cell, indicating that the ALD process on the cathode does not influence the utilization of active material. For the ALD modified LNMO electrode, the cycling retention reaches 75.3% after 300 cycles, while the unmodified sample only exhibits 46.3%. The unmodified LNMO full cell suffers from low Coulombic efficiency, and the value hardly exceeds 99.7%. Meanwhile, the ALD modified LNMO enables high Coulombic efficiency during the whole testing period. The value increases to 99.8% within 30 cycles and then reaches 99.9% after 100 cycles. Noted that the CEs from the full cell using ALD modified cathode still take more than 100 cycles to reach 99.9%, indicating the complexity of the high voltage system. Other components inside the cell are yet to be optimized. The unmodified and ALD modified LNMO cathodes were also evaluated in full cells at high temperature (55°C), as shown in Figure S6. The modified LNMO full cell de-

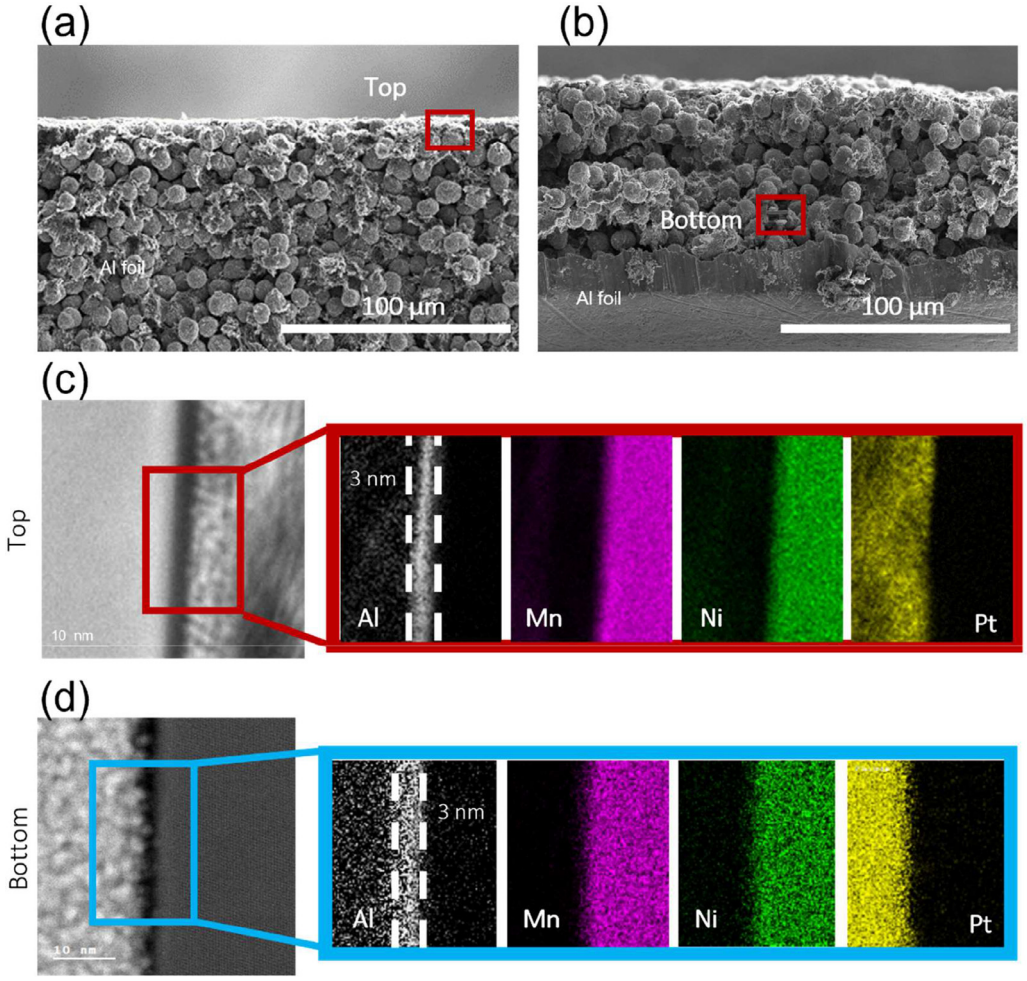

Fig. 1. Cross section images of (a) top and (b) bottom locations from a 3 mAh/cm^2 ALD modified LNMO electrode for FIB lift-out process; the STEM images with the corresponding EDS mappings from (c) the top and (d) bottom position.

livers better cycling stability than the unmodified one, which is consistent with the room temperature testing results. Considering the baseline electrolyte (Gen2) was adopted here, further optimization should focus more on electrolyte design. The average charge and discharge voltage are shown in Fig. 2(b). The unmodified LNMO in the full cell shows a growing overpotential along with the cycles. The overpotential of ALD modified LNMO in the full cell is stable even after 300 cycles. The selected charge-discharge profiles and the corresponding dQ/dV plots are shown in Figure S7 and Fig. 2(c) and (d). The oxidative peaks from the unmodified LNMO cell shift towards the higher voltage value, with a clear increasing trend in both peaks around 4.5 V (Ni^{2+}/Ni^{3+} redox) and 4.7 V (Ni^{3+}/Ni^{4+} redox). At the same time, the reductive peaks move towards the lower voltage side. The oxidative and reductive peak positions from the ALD modified LNMO full cell are well maintained. These results indicate the dramatic impedance rising and severe Li inventory loss in the full cell with the unmodified LNMO cathode. EIS measurements were further conducted to verify the cell level impedance change along with cycling, and the results are shown in Fig. 2(e) and (f). Though the initial impedance of the unmodified LNMO cell was slightly lower than the ALD modified cell, the value grew significantly as the cycle numbers increased. As for the ALD modified LNMO cell, the negligible impedance change within 200 cycles confirms the cell stability. Detailed equivalent circuit model and related fitted data are shown in Figure S8 and Table S1-S2.

To pinpoint the mechanism for performance improvement through ALD modification, post-mortem analysis was conducted on the LNMO cathode and graphite anode after 300 cycles. The cycled electrode was collected from the disassembled full cell. Two lamellas from the top and bottom parts of the cycled LNMO electrode were lifted out through the FIB process for STEM-EDS characterizations. The results are shown in Fig. 3(a) and (b). The surface modification layer with the Al signal can be well-identified at both locations based on the EDS mapping, and the thickness remains ~3 nm. Note that the modification layer becomes less conformal after long-term cycling compared to the pristine state. Additionally, we observe that both Mn and Ni distributions are inhomogeneous from the sub-surface region to the bulk area of the LNMO particle, indicating the dissolution of the transition metal ions. The inhomogeneous distribution is more evident for the top lamella, suggesting the top part of the thick electrodes suffers more from the electrolyte corrosion. This trend is not surprising considering the excess amount of electrolyte was injected from the top surface of the thick electrode during cell assembly. The surface phase changes from both the top and bottom lamellas were checked via atomic-resolution STEM, as shown in Figure S9. The results suggest that the region for phase change is within 5 nm from the surface for both top and bottom lamellas, while the top has a slightly larger phase change region than the bottom. Considering the size of the primary particles, the phase change is negligible in the presence of modification layer.

XPS was performed on both unmodified and ALD modified LNMO before and after cycling to decipher the chemical bonding information of CEI. A mild etching process was also applied on the cycled samples for depth profiling information. The corresponding results are shown in

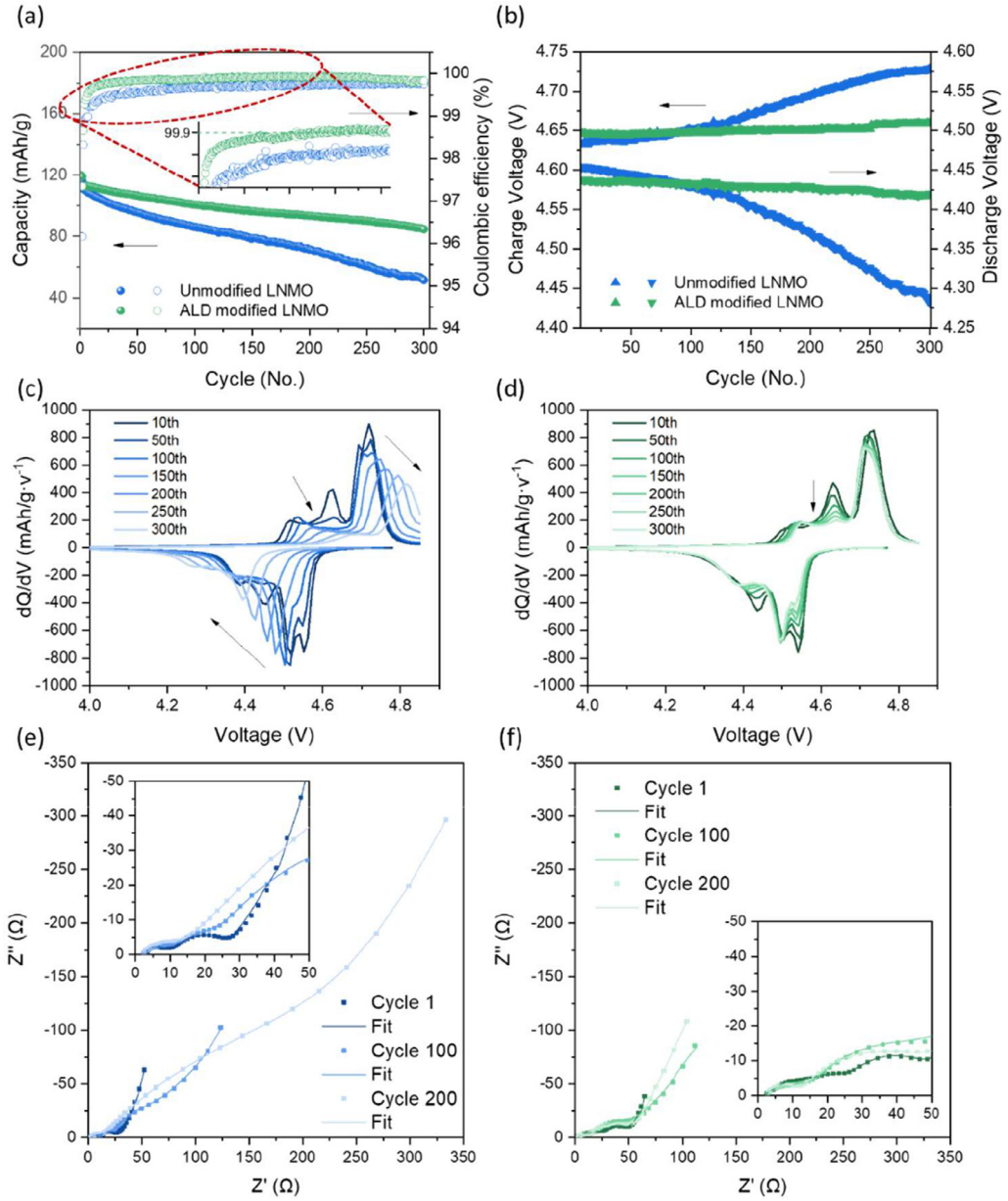

Fig. 2. Electrochemical performance comparison between the unmodified LNMO and ALD modified LNMO thick electrodes: (a) cycling performance with Coulombic efficiencies, (b) corresponding average charge and discharge voltages; the dQ/dV plots of (c) unmodified LNMO and (d) ALD modified LNMO cycled in the full cell; the Nyquist plots of (e) unmodified LNMO and (f) ALD modified LNMO full cells.

Fig. 4 for C 1s, O 1s, and Al 2p spectra, and the F 1s and P 2p spectra are shown in Figure S10. Before cycling, the unmodified LNMO electrode shows C-C bonding at 284.6 eV from the carbon-based conductive agent and the adventitious C-C/C-H bonding from surface oxides absorption. Peaks from 285 eV to 289 eV can be assigned to different carbon-oxide bonding types, usually attributed to the functional group at the edge of the conductive agent and the PVDF binder [48,49]. O 1s spectra also show evident C-O/C=O bonding and a prominent lattice oxygen peak at 530 eV. C-F peak appears in F 1s due to the PVDF presence, while no P 2p peak can be identified.

As shown in Fig. 4(b), the ALD modified LNMO electrode shows similar C 1s spectra as the unmodified sample with lower intensity at C-O/C=O and C-F peaks. The O 1s peak shows apparent differences between these two samples. The ALD modified LNMO shows a prominent peak at 530.9 eV, corresponding to the Al-O bonding. A prominent Al 2p peak at 74.0 eV and the symmetrical peak shape indicate only one kind of Al bonding presence. This evidence, combined with the STEM-EDS results shown in the previous section, confirms a uniform Al_2O_3 artificial layer on the surface of the LNMO electrode after the ALD process. After electrochemical cycling, the XPS spectra from unmodified LNMO in Fig. 4(a) show a minimal change from the C 1s spectra. In comparison, the lattice oxygen peak could still be detected from O 1s spectra and became even more apparent after the mild etching process. This indicates the CEI is not well-formed to fully cover the LNMO surface. As for the ALD modified LNMO electrode, the C 1s spectra changes drastically. The distinct rising of the C-O peak shows the accumulated organic species layer in the CEI. The O 1s peak is similar to the modified electrode before cycling, except for some shift towards the left side. This could be due to the mild corrosion between electrode and electrolyte, with $LiPF_6$ salt decomposition products forming P-O-F species. The Al 2p peak of the ALD LNMO sample shifts towards higher binding energy after cycling because of the fluorination of Al-O, which results in Al-F/Al-O-F

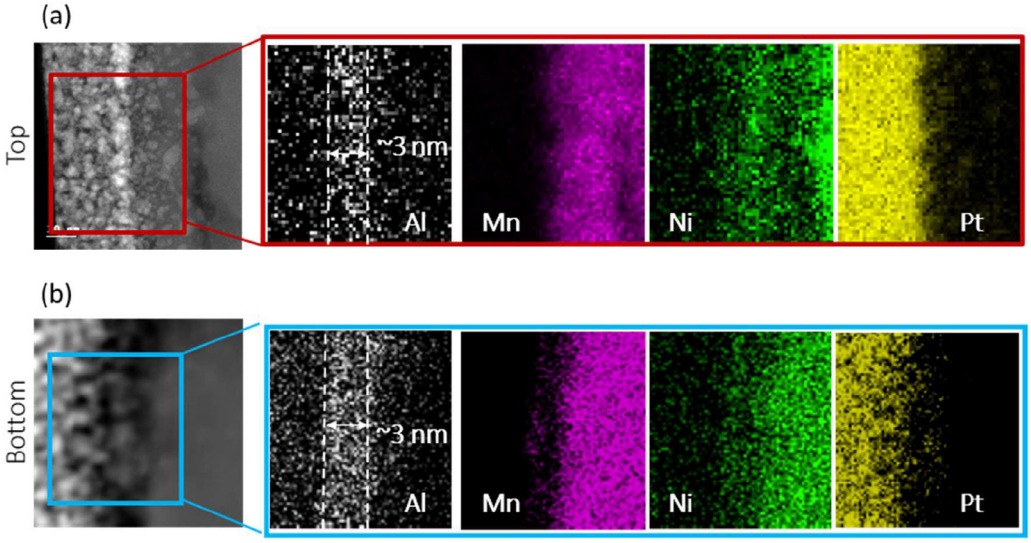

Fig. 3. The STEM images with the corresponding EDS mappings of the lamellas from the cycled LNMO electrode with ALD modification: (a) top and (b) bottom position.

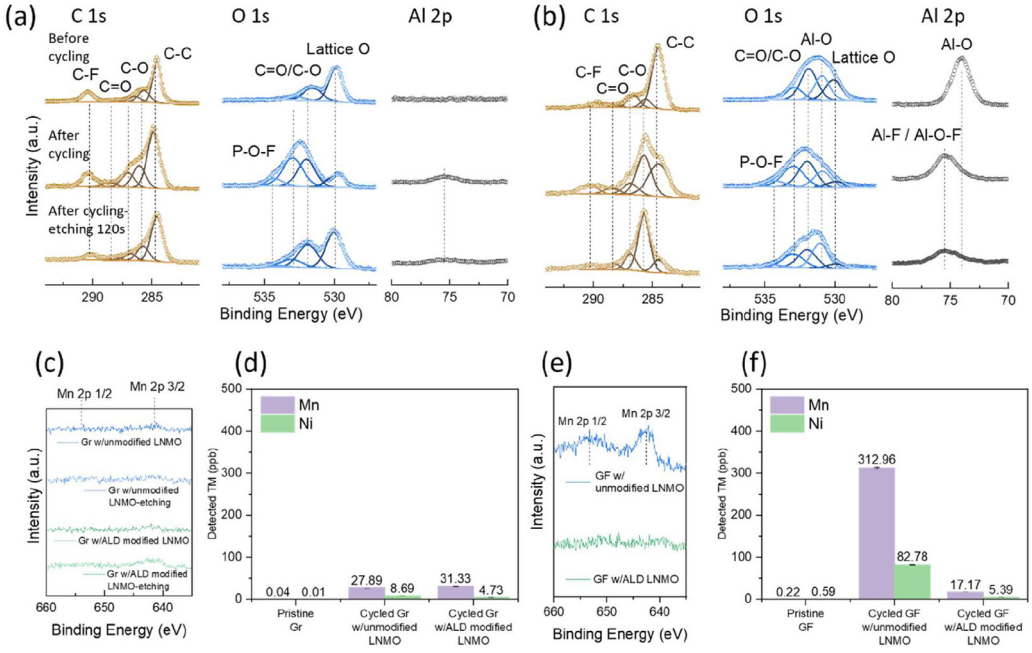

Fig. 4. XPS spectra of C 1s, O 1s and Al 2p from (a) unmodified LNMO and (b) ALD modified LNMO electrodes before and after cycling; (c) XPS spectra of Mn 2p and (d) ICP results from cycled graphite electrodes; (e) XPS spectra of Mn 2p and (f) ICP results from glass fiber separators after cycling.

bonding (≥75.5 eV). The unmodified LNMO also shows a small bump at the same binding energy, almost disappearing after the mild etching process. This Al signal could be attributed to the Al current collector corrosion. When the same etching process was applied on the cycled ALD LNMO, the Al 2p peak is still present with less intensity, implying the robustness of the Al-F/Al-O-F layer in CEI. The F 1s and P 2p spectra of the two cycled electrodes have subtle differences, indicating a similar decomposition pathway for $LiPF_6$ salt with or without the Al_2O_3 artificial surface layer. In short, the electrolyte decomposition is unavoidable considering the LNMO electrode was cycled with a high voltage range up to 4.85 V. The CEI corrosion during the high voltage cycling could be a severe problem, leading to the transition metal dissolution. The artificial CEI provided by the ALD process could effectively protect the LNMO, while the unmodified LNMO suffered direct exposure towards the degraded electrolyte.

Considering that the Al-contained CEI is robust during long-term cycling, corrosion between decomposed electrolyte and cathode should be mitigated. SEM with EDS, XPS, and ICP characterizations were performed to track Mn and Ni dissolution/redeposition on the glass fiber separators and graphite electrodes. As shown in Figure S11, both the cathode and anode show similar morphology after the long-term cycling. A negligible glass fiber residual can be identified on the cathode side, while the anodes offer clear glass fiber residue (morphology of pristine glass fiber is shown in Figure S12). A similar amount of Mn and Ni was found on both graphite anodes based on the EDS quantification (See details in Table S3). Further XPS characterizations on the cycled samples show that the Mn 2p peaks from the SEI layer of both graphite electrodes have similar intensity, as shown in Fig. 4(c). The depth profiling by Ar etching on both cycled graphite samples confirm that the Mn ions are a minor component of the SEI. ICP measurements

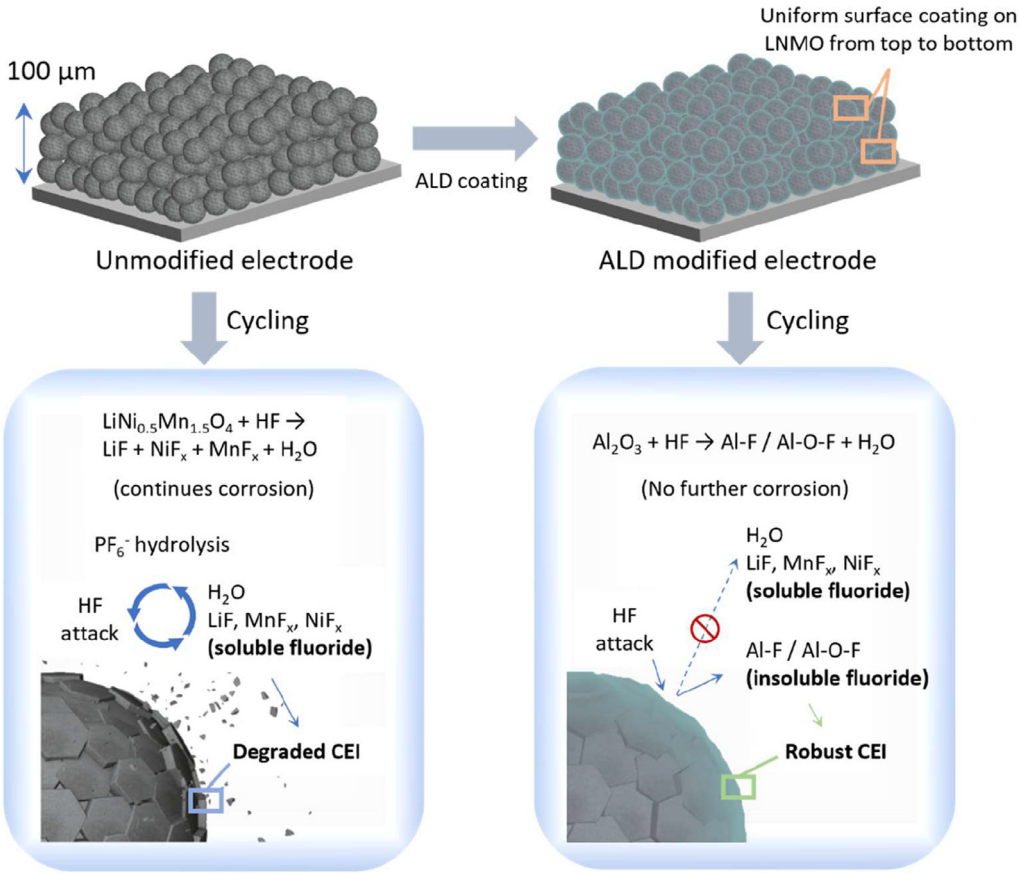

Fig. 5. Schematics of performance improvement of LNMO electrode with artificial surface layer through ALD process.

were then conducted on both graphite electrodes to quantify the total Mn and Ni dissolved from the cathode and redeposited on the graphite. As shown in Fig. 4(d), an equal increment of Mn and Ni concentration is detected for both graphite electrodes after long-term cycling. Besides the graphite anode, electrolytes should also be considered from the cycled cells. Thus, the glass fiber separators paired with different cathode samples were characterized using XPS, ICP, and SEM-EDS. The results are shown in Fig. 4(e-f) and Figure S13. The glass fiber from the unmodified LNMO cell shows obvious peaks in XPS Mn 2p spectra compared with the ALD modified LNMO cell. ICP quantification results in Fig. 4(f) further demonstrate that the unmodified LNMO has a severe Mn and Ni dissolution issue. Most of the dissolved transition metal ions are trapped in the glass fiber separator, as shown in Figure S14(e).

The above results suggest that the artificial surface layer drastically reduces the transition metal dissolution from the cathode. The electrolyte of unmodified LNMO with graphite cells degraded quickly, resulting in the increase of Mn/Ni concentration and the moisture level from the beginning cycle. Details are shown in Figure S14 and Figure S15 for the cycled electrodes and glassfiber separator collected from single layer pouch cells. The source of the moisture is well documented in the literature that the common carbonate electrolyte solvents such as ethylene carbonate would be dehydrogenated, where the free protons would be released [50,51]. These protons would attack the cathode materials, which results in moisture generation. Then $LiPF_6$ salt would be hydrolyzed to generate HF, thus further corroding the materials inside the cells. The possible products from these parasitic reactions include different metal fluorides, such as LiF, MnF_x, and NiF_x. However, all these fluorides are soluble in the presence of HF; [52] thus, the cathode interphase would never be stabilized. The side products would also clog the lithium-ion diffusion pathway in between the cathode and anode, leading to the gradual growth of the cell level impedance. For the ALD modified LNMO electrode, the artificial Al_2O_3 interphase would be corroded by HF at the beginning. The generated Al-F/Al-O-F would not be corroded further due to its inertness towards HF and insolubility in water and HF solution [52]. And as a result, the converted artificial interphase can be well remained on the cathode surface during long-term cycling, thus providing constant protection of LNMO materials so that both Mn and Ni can hardly be detected either in the glass fiber separator or the graphite anode. Therefore, the cathode active material LNMO can be well preserved by the artificial interphase. The long-term cycling of LNMO-graphite cells with high areal loading can be improved — the performance improvement mechanism through ALD modification is illustrated in Fig. 5.

In conclusion, the feasibility of surface modification by the ALD process on the LNMO thick electrode (up to 100 μm) has been verified. The lamellas lifted out from the thick electrode's top and bottom locations have been checked by STEM-EDS, and the Al signal is present at both locations. The conductive agent and the binder have also been carefully checked that the surfaces can be partially coated via the ALD process, which may mitigate the parasitic reaction. Further optimization of the ALD process may bring opportunities to modify even thicker electrodes with other functional compounds. The whole experimental verification process provides an example for surface coating uniformity and stability study. Only with thorough examination can the ALD coating method be with high-quality control for industrial-level applications. Similar verification procedure can be extended to thick electrodes using cathode materials such as layered NCM and $LiCoO_2$. The cycling stability of ALD modified LNMO cathode with 3 mAh/cm^2 areal capacity has been greatly improved under the high voltage operating conditions, without sacrificing the specific capacity of cathode material. Though the Al_2O_3 is converted to Al-F/Al-O-F species with a less conformal surface coverage after long-term cycling, the thickness of the artificial surface layer

is well maintained. The existence of the robust surface layer reduces the active materials' corrosion from the degraded electrolyte, and the TM dissolution amount is thus mitigated. These findings demonstrate the importance of interphase protection for high voltage cathode materials to achieve long-term cycling stability.

Declaration of Competing interest

The authors declare that they have no known competing financial interests or personal relationships that could have appeared to influence the work reported in this paper.

CRediT authorship contribution statement

Weikang Li: Methodology, Validation, Writing – original draft. **Diyi Cheng:** Methodology, Investigation. **Ryosuke Shimizu:** Investigation. **Yixuan Li:** Investigation. **Weiliang Yao:** Investigation. **Ganesh Raghavendran:** Investigation. **Minghao Zhang:** Writing – review & editing. **Ying Shirley Meng:** Writing – review & editing, Supervision.

Acknowledgment

This work was supported by the Office of Vehicle Technologies of the US Department of Energy and U.S. Department of the Army's Tank & Automotive Research Development and Engineering Command (TARDEC) through the Battery R&D program under contract DE-EE0008442. FIB-SEM, XRD, and SEM were performed at the San Diego Nanotechnology Infrastructure, a member of the National Nanotechnology Coordinated Infrastructure supported by the US National Science Foundation (NSF) (grant ECCS-1542148). The authors acknowledge the use of facilities and instrumentation at the UC Irvine Materials Research Institute (IMRI), which is supported in part by the National Science Foundation through the UC Irvine Materials Research Science and Engineering Center (DMR-2011967), Specifically, the XPS work was performed using instrumentation funded in part by the National Science Foundation Major Research Instrumentation Program under grant No. CHE-1338173. The authors acknowledge Neware Instruments for the Neware battery test system.

Supplementary materials

Supplementary material associated with this article can be found, in the online version, at doi:10.1016/j.ensm.2022.04.002.

References

[1] J. Liu, Z. Bao, Y. Cui, E.J. Dufek, J.B. Goodenough, P. Khalifah, Q. Li, B.Y. Liaw, P. Liu, A. Manthiram, Y.S. Meng, V.R. Subramanian, M.F. Toney, V.V. Viswanathan, M.S. Whittingham, J. Xiao, W. Xu, J. Yang, X.Q. Yang, J.G. Zhang, Pathways for Practical High-Energy Long-Cycling Lithium Metal Batteries, Nature Energy (2019) 180–186 Nature Publishing Group March 1, doi:10.1038/s41560-019-0338-x.

[2] R. Schmuch, R. Wagner, G. Hörpel, T. Placke, M. Winter, G. Horpel, T. Placke, M. Winter, Performance and Cost of Materials for Lithium-Based Rechargeable Automotive Batteries, Nat. Energy 3 (4) (2018) 267–278, doi:10.1038/s41560-018-0107-2.

[3] F. Duffner, N. Kronemeyer, J. Tübke, J. Leker, M. Winter, R. Schmuch, Post-Lithium-Ion Battery Cell Production and Its Compatibility with Lithium-Ion Cell Production Infrastructure, *Nature Energy*. Nature Research (2021) 123–134 February 1, doi:10.1038/s41560-020-00748-8.

[4] W. Li, E.M. Erickson, A. Manthiram, High-Nickel Layered Oxide Cathodes for Lithium-Based Automotive Batteries, Nat. Energy 5 (1) (2020) 26–34, doi:10.1038/s41560-019-0513-0.

[5] W. Li, Y.G. Cho, W. Yao, Y. Li, A. Cronk, R. Shimizu, M.A. Schroeder, Y. Fu, F. Zou, V. Battaglia, A. Manthiram, M. Zhang, Y.S. Meng, Enabling High Areal Capacity for Co-Free High Voltage Spinel Materials in next-Generation Li-Ion Batteries, J. Power Sources 473 (April) (2020) 228579, doi:10.1016/j.jpowsour.2020.228579.

[6] X. Yu, Releasing Oxygen from the Bulk, Nat. Energy 6 (6) (2021) 572–573, doi:10.1038/s41560-021-00834-5.

[7] G. Liang, V.K. Peterson, K.W. See, Z. Guo, W.K. Pang, Developing High-Voltage Spinel LiNi0.5Mn1.5O4 Cathodes for High-Energy-Density Lithium-Ion Batteries: Current Achievements and Future Prospects, J. Mater. Chem. A 8 (31) (2020) 15373–15398, doi:10.1039/d0ta02812f.

[8] T. Yoon, J. Soon, T.J. Lee, J.H. Ryu, S.M. Oh, Dissolution of Cathode–Electrolyte Interphase Deposited on LiNi0.5Mn1.5O4 for Lithium-Ion Batteries, J. Power Sources 503 (2021) 230051, doi:10.1016/j.jpowsour.2021.230051.

[9] K. Kim, H. Ma, S. Park, N.-S. Choi, Electrolyte-Additive-Driven Interfacial Engineering for High-Capacity Electrodes in Lithium-Ion Batteries: Promise and Challenges, ACS Energy Lett 5 (5) (2020) 1537–1553, doi:10.1021/acsenergylett.0c00468.

[10] K. Xu, Electrolytes and Interphases in Li-Ion Batteries and Beyond, Chem. Rev. 114 (23) (2014) 11503–11618, doi:10.1021/cr500003w.

[11] M. Liu, J. Vatamanu, X. Chen, L. Xing, K. Xu, W. Li, Hydrolysis of LiPF 6 - Containing Electrolyte at High Voltage, ACS Energy Lett 6 (6) (2021) 2096–2102, doi:10.1021/acsenergylett.1c00707.

[12] F. De Giorgio, N. Laszczynski, J. von Zamory, M. Mastragostino, C. Arbizzani, S. Passerini, Graphite//LiNi0.5 Mn1.5 O4 Cells Based on Environmentally Friendly Made-in-Water Electrodes, ChemSusChem 10 (2) (2017) 379–386, doi:10.1002/cssc.201601249.

[13] G. Liang, Z. Wu, C. Didier, W. Zhang, J. Cuan, B. Li, K.Y. Ko, P.Y. Hung, C.Z. Lu, Y. Chen, G. Leniec, S.M. Kaczmarek, B. Johannessen, L. Thomsen, V.K. Peterson, W.K. Pang, Z. Guo, A Long Cycle-Life High-Voltage Spinel Lithium-Ion Battery Electrode Achieved by Site-Selective Doping, Angew. Chemie - Int. Ed. 59 (26) (2020) 10594–10602, doi:10.1002/anie.202001454.

[14] S.R. Li, C.H. Chen, J.R Dahn, Studies of LiNi 0.5 Mn 1.5 O 4 as a Positive Electrode for Li-Ion Batteries: M 3+ Doping (M = Al, Fe, Co and Cr), Electrolyte Salts and LiNi 0.5 Mn 1.5 O 4 /Li 4 Ti 5 O 12 Cells, J. Electrochem. Soc. 160 (11) (2013) A2166–A2175, doi:10.1149/2.075311jes.

[15] J. Alvarado, M.A. Schroeder, M. Zhang, O. Borodin, E. Gobrogge, M. Olguin, M.S. Ding, M. Gobet, S. Greenbaum, Y.S. Meng, K.A Xu, Carbonate-Free, Sulfone-Based Electrolyte for High-Voltage Li-Ion Batteries, Mater. Today 21 (4) (2018) 341–353, doi:10.1016/j.mattod.2018.02.005.

[16] A. Hofmann, A. Höweling, N. Bohn, M. Müller, J.R. Binder, T. Hanemann, Additives for Cycle Life Improvement of High-Voltage LNMO-Based Li-Ion Cells, ChemElectroChem 6 (20) (2019) 5255–5263, doi:10.1002/celc.201901120.

[17] T. Yang, H. Zeng, W. Wang, X. Zhao, W. Fan, C. Wang, X. Zuo, R. Zeng, J. Nan, Lithium Bisoxalatodifluorophosphate (LiBODFP) as a Multifunctional Electrolyte Additive for 5 v LiNi0.5Mn1.5O4-Based Lithium-Ion Batteries with Enhanced Electrochemical Performance, J. Mater. Chem. A 7 (14) (2019) 8292–8301, doi:10.1039/c9ta01293a.

[18] M. Hallot, B. Caja-Munoz, C. Leviel, O.I. Lebedev, R. Retoux, J. Avila, P. Roussel, M.C. Asensio, C. Lethien, Atomic Layer Deposition of a Nanometer-Thick Li3PO4Protective Layer on LiNi0.5Mn1.5O4Films: Dream or Reality for Long-Term Cycling? ACS Appl. Mater. Interfaces 13 (13) (2021) 15761–15773, doi:10.1021/acsami.0c21961.

[19] H.M. Cho, M. Chen, A.C. V; MacRae, Y.S. Meng, Effect of Surface Modification on Nano-Structured LiNi(0.5)Mn(1.5)O4 Spinel Materials, ACS Appl Mater Interfaces 7 (30) (2015) 16231–16239, doi:10.1021/acsami.5b01392.

[20] T. Hwang, J.K. Lee, J. Mun, W. Choi, Surface-Modified Carbon Nanotube Coating on High-Voltage LiNi0.5Mn1.5O4 Cathodes for Lithium Ion Batteries, J. Power Sources 322 (2016) 40–48, doi:10.1016/j.jpowsour.2016.04.118.

[21] S.H. Jung, D.H. Kim, P. Brüner, H. Lee, H.J. Hah, S.K. Kim, Y.S. Jung, Extremely Conductive RuO2-Coated LiNi0.5Mn1.5O4 for Lithium-Ion Batteries, Electrochim. Acta 232 (2017) 236–243, doi:10.1016/j.electacta.2017.02.109.

[22] C.T. Chu, A. Mondal, N.V. Kosova, J.Y. Lin, Improved High-Temperature Cyclability of AlF3 Modified Spinel LiNi0.5Mn1.5O4 Cathode for Lithium-Ion Batteries, Appl. Surf. Sci. 530 (2020) 147169, doi:10.1016/j.apsusc.2020.147169.

[23] M. Kuenzel, G.T. Kim, M. Zarrabeitia, S.D. Lin, A.R. Schuer, D. Geiger, U. Kaiser, D. Bresser, S. Passerini, Crystal Engineering of TMPOx-Coated LiNi0.5Mn1.5O4 Cathodes for High-Performance Lithium-Ion Batteries, Mater. Today 39 (xx) (2020) 127–136, doi:10.1016/j.mattod.2020.04.003.

[24] L. Chen, R.E. Warburton, K.S. Chen, J.A. Libera, C. Johnson, Z. Yang, M.C. Hersam, J.P. Greeley, J.W. Elam, Mechanism for Al2O3 Atomic Layer Deposition on LiMn2O4 from In Situ Measurements and Ab Initio Calculations, Chem 4 (10) (2018) 2418–2435, doi:10.1016/j.chempr.2018.08.006.

[25] I.D. Scott, Y.S. Jung, A.S. Cavanagh, Y. Yan, A.C. Dillon, S.M. George, S.H. Lee, Ultrathin Coatings on Nano-LiCoO2 for Li-Ion Vehicular Applications, Nano Lett 11 (2) (2011) 414–418, doi:10.1021/nl1030198.

[26] J.T. Lee, F.M. Wang, C.S. Cheng, C.C. Li, C.H. Lin, Low-Temperature Atomic Layer Deposited Al2O3 Thin Film on Layer Structure Cathode for Enhanced Cycleability in Lithium-Ion Batteries, Electrochim. Acta 55 (12) (2010) 4002–4006, doi:10.1016/j.electacta.2010.02.043.

[27] Dongsheng Guan, A. Jeevarajan, J. Ying Wang, Enhanced Cycleability of LiMn2O4 Cathodes by Atomic Layer Deposition of Nanosized-Thin Al2O3 Coatings, Nanoscale 3 (4) (2011) 1465–1469, doi:10.1039/C0NR00939C.

[28] G.H. Waller, P.D. Brooke, B.H. Rainwater, S.Y. Lai, R. Hu, Y. Ding, F.M. Alamgir, K.H. Sandhage, M.L. Liu, Structure and Surface Chemistry of Al2O3 Coated LiMn2O4 Nanostructured Electrodes with Improved Lifetime, J. Power Sources 306 (2016) 162–170, doi:10.1016/J.JPOWSOUR.2015.11.114.

[29] L.A. Riley, S. Van Atta, A.S. Cavanagh, Y. Yan, S.M. George, P. Liu, A.C. Dillon, S.H. Lee, Electrochemical Effects of ALD Surface Modification on Combustion Synthesized LiNi1/3Mn1/3Co1/3O2 as a Layered-Cathode Material, J. Power Sources 196 (6) (2011) 3317–3324, doi:10.1016/j.jpowsour.2010.11.124.

[30] D. Mohanty, K. Dahlberg, D.M. King, L.A. David, A.S. Sefat, D.L. Wood, C. Daniel, S. Dhar, V. Mahajan, M. Lee, F. Albano, Modification of Ni-Rich FCG NMC and NCA Cathodes by Atomic Layer Deposition: Preventing Surface Phase Transitions for High-Voltage Lithium-Ion Batteries, Sci. Rep. 6 (February) (2016) 1–16, doi:10.1038/srep26532.

[31] X. Zhang, I. Belharouak, L. Li, Y. Lei, J.W. Elam, A. Nie, X. Chen, R.S. Yassar, R.L. Axelbaum, Structural and Electrochemical Study of Al2O3 and TiO2 Coated

Li1.2Ni0.13Mn0.54Co0.13O2 Cathode Material Using ALD, Adv. Energy Mater. 3 (10) (2013) 1299–1307, doi:10.1002/aenm.201300269.
[32] Y. Seok Jung, A.S. Cavanagh, Y. Yan, S.M. George, A Manthiram, Effects of Atomic Layer Deposition of Al2O3 on the Li [Li0.20Mn0.54Ni0.13Co0.13]O2 Cathode for Lithium-Ion Batteries, J. Electrochem. Soc. 158 (12) (2011) A1298, doi:10.1149/2.030112jes.
[33] Y.S. Jung, A.S. Cavanagh, L.A. Riley, S.H. Kang, A.C. Dillon, M.D. Groner, S.M. George, S.H. Lee, Ultrathin Direct Atomic Layer Deposition on Composite Electrodes for Highly Durable and Safe Li-Ion Batteries, Adv Mater 22 (19) (2010) 2172–2176, doi:10.1002/adma.200903951.
[34] X. Fang, M. Ge, J. Rong, Y. Che, N. Aroonyadet, X. Wang, Y. Liu, A. Zhang, C. Zhou, Ultrathin Surface Modification by Atomic Layer Deposition on High Voltage Cathode LiNi0.5Mn1.5O4 for Lithium Ion Batteries, Energy Technol 2 (2) (2014) 159–165, doi:10.1002/ente.201300102.
[35] J. Song, X. Han, K.J. Gaskell, K. Xu, S.B. Lee, L. Hu, Enhanced Electrochemical Stability of High-Voltage LiNi0.5Mn1.5O4 Cathode by Surface Modification Using Atomic Layer Deposition, J. Nanoparticle Res. 16 (11) (2014) 1–8, doi:10.1007/s11051-014-2745-z.
[36] A. Kraytsberg, H. Drezner, M. Auinat, A. Shapira, N. Solomatin, P. Axmann, M. Wohlfahrt-Mehrens, Y. Ein-Eli, Atomic Layer Deposition of a Particularized Protective MgF2 Film on a Li-Ion Battery LiMn1.5Ni0.5O4 Cathode Powder Material, ChemNanoMat 1 (8) (2015) 577–585, doi:10.1002/cnma.201500149.
[37] H.M. Cho, M.V. Chen, A.C. MacRae, Y.S. Meng, Effect of Surface Modification on Nano-Structured LiNi0.5Mn1.5O4 Spinel Materials, ACS Appl. Mater. Interfaces 7 (30) (2015) 16231–16239, doi:10.1021/acsami.5b01392.
[38] B. Xiao, J. Liu, Q. Sun, B. Wang, M.N. Banis, D. Zhao, Z. Wang, R. Li, X. Cui, T.-K. Sham, X. Sun, Unravelling the Role of Electrochemically Active FePO4 Coating by Atomic Layer Deposition for Increased High-Voltage Stability of LiNi0.5Mn1.5O4 Cathode Material, Adv. Sci. 2 (5) (2015) 1500022, doi:10.1002/ADVS.201500022.
[39] X. Fang, F. Lin, D. Nordlund, M. Mecklenburg, M. Ge, J. Rong, A. Zhang, C. Shen, Y. Liu, Y. Cao, M.M. Doeff, C. Zhou, Atomic Insights into the Enhanced Surface Stability in High Voltage Cathode Materials by Ultrathin Coating, Adv. Funct. Mater. 27 (7) (2017) 1602873, doi:10.1002/adfm.201602873.
[40] B. Xiao, H. Liu, J. Liu, Q. Sun, B. Wang, K. Kaliyappan, Y. Zhao, M.N. Banis, Y. Liu, R. Li, T.K. Sham, G.A. Botton, M. Cai, X. Sun, Nanoscale Manipulation of Spinel Lithium Nickel Manganese Oxide Surface by Multisite Ti Occupation as High-Performance Cathode, Adv Mater 29 (47) (2017) 1703764, doi:10.1002/adma.201703764.
[41] J. Li, Y. Gao, X. Liang, J. Park, Ultra-Thin Coating and Three-Dimensional Electrode Structures to Boosted Thick Electrode Lithium-Ion Battery Performance, Batter. Supercaps 2 (2) (2019) 139–143, doi:10.1002/batt.201800091.
[42] O. Tiurin, N. Solomatin, M. Auinat, Y. Ein-Eli, Atomic Layer Deposition (ALD) of Lithium Fluoride (LiF) Protective Film on Li-Ion Battery LiMn1.5Ni0.5O4 Cathode Powder Material, J. Power Sources 448 (2020) 227373, doi:10.1016/j.jpowsour.2019.227373.
[43] X. Xiao, D. Ahn, Z. Liu, J.H. Kim, P. Lu, Atomic Layer Coating to Mitigate Capacity Fading Associated with Manganese Dissolution in Lithium Ion Batteries, Electrochem. commun. 32 (2013) 31–34, doi:10.1016/j.elecom.2013.03.030.
[44] J.S. Park, X. Meng, J.W. Elam, S. Hao, C. Wolverton, C. Kim, J. Cabana, Ultrathin Lithium-Ion Conducting Coatings for Increased Interfacial Stability in High Voltage Lithium-Ion Batteries, Chem. Mater. 26 (10) (2014) 3128–3134, doi:10.1021/cm500512n.
[45] J.W.H. Kim, D.H. Kim, D.Y. Oh, H. Lee, J.W.H. Kim, J.H. Lee, Y.S. Jung, Surface Chemistry of LiNi0.5Mn1.5O4 Particles Coated by Al2O3 Using Atomic Layer Deposition for Lithium-Ion Batteries, J. Power Sources 274 (2015) 1254–1262, doi:10.1016/j.jpowsour.2014.10.207.
[46] A. Shapira, O. Tiurin, N. Solomatin, M. Auinat, A. Meitav, Y. Ein-Eli, Robust AlF3 Atomic Layer Deposition Protective Coating on LiMn1.5Ni0.5O4 Particles: An Advanced Li-Ion Battery Cathode Material Powder, ACS Appl. Energy Mater. 1 (12) (2018) 6809–6823, doi:10.1021/acsaem.8b01048.
[47] Y. Gao, H. Yu, P. Sandineni, X. He, A. Choudhury, J. Park, X. Liang, Fe Doping in LiMn1.5Ni0.5O4by Atomic Layer Deposition Followed by Annealing: Depths and Occupation Sites, J. Phys. Chem. C 125 (14) (2021) 7560–7567, doi:10.1021/acs.jpcc.1c00225.
[48] F. Wu, W. Li, L. Chen, Y. Su, L. Bao, W. Bao, Z. Yang, J. Wang, Y. Lu, S. Chen, Renovating the Electrode-Electrolyte Interphase for Layered Lithium- & Manganese-Rich Oxides, Energy Storage Mater 28 (2020) 383–392, doi:10.1016/j.ensm.2019.12.017.
[49] A.N. Mansour, D.G. Kwabi, R.A. Quinlan, Y.-C. Lu, Y. Shao-Horn, Probing the Electrode-Electrolyte Interface in Cycled LiNi0.5Mn1.5O4by XPS Using Mg and Synchrotron X-Rays, J. Electrochem. Soc. 163 (14) (2016) A2911–A2918, doi:10.1149/2.0331614jes.
[50] Y. Yu, P. Karayaylali, Y. Katayama, L. Giordano, M. Gauthier, F. Maglia, R. Jung, I. Lund, Y. Shao-Horn, Coupled LiPF6 Decomposition and Carbonate Dehydrogenation Enhanced by Highly Covalent Metal Oxides in High-Energy Li-Ion Batteries, J. Phys. Chem. C 122 (48) (2018) 27368–27382, doi:10.1021/acs.jpcc.8b07848.
[51] Y. Zhang, Y. Katayama, R. Tatara, L. Giordano, Y. Yu, D. Fraggedakis, J.G. Sun, F. Maglia, R. Jung, M.Z. Bazant, Y. Shao-Horn, Revealing Electrolyte Oxidation: Via Carbonate Dehydrogenation on Ni-Based Oxides in Li-Ion Batteries by in Situ Fourier Transform Infrared Spectroscopy, Energy Environ. Sci. 13 (1) (2020) 183–199, doi:10.1039/c9ee02543j.
[52] A.W. Jache, G.H. Cady, Solubility of Fluorides of Metals in Liquid Hydrogen Fluoride, J. Phys. Chem. 56 (9) (1952) 1106–1109, doi:10.1021/j150501a018.